WSS/CI 96S-006

Oxygen Atom Concentrations and NO Production Rates in a Turbulent H_2/N_2 Jet Flame

R. S. Barlow, G. J. Fiechtner
Combustion Research Facility
Sandia National Laboratories
Livermore, CA 94551-0969

J.-Y. Chen
Department of Mechanical Engineering
University of California
Berkeley, CA 49720

Presented at the 1996 Spring Meeting of the
Western States Section/The Combustion Institute
Arizona State University, Tempe, Arizona, March 11-12, 1996

Sandia National Laboratories

Oxygen Atom Concentrations and NO Production Rates in a Turbulent H_2/N_2 Jet Flame

R. S. Barlow, G. J. Fiechtner
Combustion Research Facility
Sandia National Laboratories
Livermore, CA 94551-0969

J.-Y. Chen
Department of Mechanical Engineering
University of California
Berkeley, CA 49720

ABSTRACT

An experimental procedure is demonstrated that allows determination of instantaneous oxygen atom concentrations and thermal NO production rates in turbulent flames. This is accomplished without direct measurement of O-atoms by laser-induced fluorescence, a technique that has been shown to be problematic. Simultaneous point measurements of temperature, the major species, OH, and NO are performed in a nonpremixed turbulent jet flame of nitrogen-diluted hydrogen fuel. The O-atom concentration for each laser shot is derived from these data, based upon the assumption of partial equilibrium of the reaction $OH+OH=O+H_2O$. The derived O-atom concentration is then used, along with the measured N_2 concentration and temperature, to calculate the instantaneous thermal (Zeldovich) NO production rate. The partial equilibrium assumption is shown to be appropriate for these specific flame conditions. Results demonstrate that the present experimental approach yields quantitative data on O-atom concentrations and thermal NO production rates in flames where the partial equilibrium assumption is valid. These data provide new insights on the effects of turbulence-chemistry interactions on thermal NO formation, and they may be used in evaluating combustion models. Experimental results are compared with steady strained laminar flame calculations and with turbulent flame predictions obtained using the Monte Carlo pdf model with detailed chemistry. The laminar flame results are not consistent with the measurements. With some exceptions there is good agreement between the pdf prediction and the experiment when results are considered in mixture-fraction coordinates (scatter plots and conditional means). Agreement is not as good when radial profiles of averaged scalars quantities are compared. This indicates that the present pdf model predicts the hydrogen and nitrogen chemistry with good accuracy, but that improvements are needed in the modeling of the turbulent fluid dynamics and mixing.

INTRODUCTION

An important goal of current research and development efforts in combustion is to minimize NO_x formation in practical combustion devices [1]. Thermal NO formation is a significant mechanism in many combustion applications, particularly those that rely upon nonpremixed flames. Considerable experimental research has been carried out using gas-sampling probes to determine the effects of parameters such as fuel type, residence time, radiation, buoyancy, and diluents on NO_x formation in jet flames [2-9]. More recently, simultaneous laser-based measurements of multiple species have been used to investigate NO formation in hydrogen jet flames [10-13], in laminar CH_4-air Bunsen flames [14], and in bluff-body-stabilized flames of various fuels [15]. In much of this work there has been speculation regarding the effects of turbulence-chemistry interactions on super-equilibrium levels of O-atoms, which contribute to thermal NO production. However, O-atom concentrations have not been measured in the context of a study of NO formation in turbulent nonpremixed flames.

Comparisons of Monte Carlo pdf and Conditional Moment Closure (CMC) model predictions of hydrogen jet flames [16] have revealed differences in O-atom levels, even though the predictions applied the same turbulence model, chemical mechanism, and radiation model. Experimental data on O-atom concentrations and thermal NO production rates would, therefore, be useful in developing a better understanding the influence of turbulence-chemistry interactions on NO formation and in evaluating various modeling approaches. Validation of models that could predict regions of high NO production (hot spots) would be particularly useful.

Investigations of laser-induced fluorescence (LIF) detection of O-atoms in laminar flames [17,18] suggest that quantitative single-shot measurements of O-atom concentrations in turbulent flames would be a difficult challenge at best. A major complication is that the 226-nm laser pulse that excites the O-atoms tends to produce additional O-atoms by photolysis. In the present study we demonstrate an experimental alternative to direct LIF measurements of O-atom concentrations in turbulent flames. Pulsed-laser diagnostics are used to obtain simultaneous point measurements of temperature, the major species concentrations, OH, and NO. The instantaneous O-atom concentration is derived from the measured temperature, [OH], and $[H_2O]$, based on the assumption of partial equilibrium of the reaction:

$$OH + OH = O + H_2O, \tag{R1}$$

such that

$$[O] = K_{EQ,1}\,[OH]^2/[H_2O]. \tag{1}$$

The thermal NO production rate is then calculated on a shot-to-shot basis as twice the forward rate of the first (rate limiting) reaction in the extended Zeldovich mechanism [1]:

$$N_2 + O \rightarrow N + NO, \tag{R2}$$

$$N + O_2 \rightarrow O + NO, \tag{R3}$$

$$N + OH \rightarrow H + NO, \tag{R4}$$

such that

$$d[NO]/dt = 2k_2\,[N_2][O], \tag{2}$$

where

$$k_2 = 1.84\times10^{11}\exp(-38730/T)\ \text{moles/liter-s}.$$

For the purpose of demonstrating this approach, the present paper focuses on results of measurements along a single radial profile in a nonpremixed turbulent jet flame of 80% H_2 and 20% N_2 by volume, with a Reynolds number of 14,000. We show that the partial equilibrium assumption is valid for these flame conditions and that the derived O-atom concentrations and NO

production rates are of useful accuracy. Experimental data are also compared with results of steady strained laminar flame calculations and a Monte Carlo pdf simulation, based only on the specified experimental boundary conditions of nozzle diameter, fuel composition, jet velocity, coflow velocity, and ambient air conditions.

EXPERIMENTAL METHODS

The flow facility, diagnostic systems, and calibration procedures have been described previously [10,11,14], and only a brief summary is included here. Spontaneous Raman scattering of the beams from two Nd:YAG lasers (532 nm) was used to measure concentrations of the major species, N_2, O_2, H_2, and H_2O. Pulse-stretching optics were used to avoid breakdown at the focus, and the energies in the beams were measured by two pyro-electric joule meters. The joule meters replace the Photodiode used in previous work, and with this modification the signal-to-noise ratio for Rayleigh signal normalized by laser energy improved to about 500:1 for measurements in wind-tunnel air. The Rayleigh scattering signal was converted to temperature using a species-weighted scattering cross section, based on the Raman measurements. Linear LIF was used to measure OH and NO, and the fluorescence signals were corrected on a shot-to-shot basis for variations in the Boltzmann fraction and the collisional quenching rate. These corrections were determined from the measured species concentrations and temperature and from published correlations for collisional quenching cross sections [19,20]. The spatial resolution for all measurements was ~750 μm in each direction.

The temperature dependent calibration functions for each of the Raman channels were determined through an extensive series of measurements in the flow above a gas heater and in flat flames above a Hencken burner [11] over a wide range of conditions of temperature and species concentrations. Radiative losses from the calibration flames are accounted for in this procedure by calculating equilibrium species concentrations at the measured Rayleigh temperature rather than the adiabatic equilibrium temperature. Additional Raman/Rayleigh calibrations were performed immediately before and after the turbulent flame measurements to allow fine tuning of calibration factors and to ensure that no significant drift of the calibrations occurred during the experiment. OH measurements were referenced to a H_2-air Hencken burner flame, where the OH number density had been measured previously by laser absorption [10]. OH calibration factors measured before and after the turbulent flame experiment agreed within 1 percent. The NO calibration factor was determined by doping a lean premixed $CH_4/O_2/N_2$ laminar flat flame (McKenna burner) with several known concentrations of NO. Detailed flame calculations have shown that destruction of the seeded NO in this flame is negligible [13]. Computer control of the calibrated flow controllers kept the flame temperature constant within ±5K as NO-doped N_2 progressively replaced the pure N_2. The NO calibrations were also performed immediately before and after the turbulent flame measurements. Resulting calibration factors differed by 4 percent, and the average of the two values was used in reducing the turbulent flame data.

Derivation of O-atom concentrations and NO production rates depends on good precision and accuracy of the measured scalars. Measurements of OH and temperature are most critical, due to the squared dependence of the derived O-atom concentration on [OH] and the high sensitivity of the NO production rate to temperature. A brief consideration of random and systematic errors is included here, and a more complete treatment of experimental uncertainties is provided elsewhere [21]. Estimates of random errors at temperatures relevant to thermal NO production were based upon the rms standard deviations of measured temperature and concentrations in steady premixed flat flames. The expected random errors (one standard deviation) in O-atom concentrations and NO production rates were estimated from Eq. (1) and Eq. (2), assuming statistical independence of errors in the measured temperature and species. These estimates are listed in Table 1 along with the conditions at which they were determined. The actual standard deviations of the [O] and

dNO/dt derived at the calibration conditions using the full data reduction procedure are listed second.

The most important potential sources of systematic error in the present experiment are: uncertainty in the OH calibration, which was estimated to be ±10%; uncertainties in the temperature-dependent Raman calibration curves, which were estimated from repeatability of calibrations, including those at the beginning and end of the experiment; and uncertainty in the Rayleigh temperature, which was also estimated from repeatability of calibrations and estimates of radiative losses from the calibration flames. Systematic uncertainties for these same quantities were also determined from Eq. (1) and Eq. (2) as the direct, worst-case products of the contributing potential systematic errors. These estimates are also given in Table 1.

Table 1 Relative standard deviations of scalars measured or derived at the listed conditions in steady premixed flat flames and potential systematic uncertainties estimated from the calibration procedures

Measured or derived scalar	Random error σ(rms)	Flame conditions (mole frac., T)	Potential systematic error
$[N_2]$	3%	0.71, 2140 K	2%
$[H_2O]$	5%	0.18, 2140 K	3%
[OH]	7%	0.0023, 2140 K	10%
[NO]	10%	26 ppm, 1740 K	10%
T	1%	2140 K	2%
[O]	15% [a], 14% [b]	2140 K	35%
d[NO]/dt	17% [a], 21% [b]	2140 K	80%

[a] Estimated by combining errors in [OH], $[H_2O]$, and T, assuming statistical independence
[b] One standard deviation in fully reduced results of measurements in a premixed CH_4-air flame

The burner was a straight tube (inner diameter, d=4.58 mm; outer diameter 6.34 mm; squared-off end) centered at the exit of a 30-cm by 30-cm vertical wind tunnel contraction. The coflow air conditions were: 0.75 ± 0.05 m/s velocity, 290 K temperature, 0.0116 mole fraction of H_2O. The fuel composition was 80% H_2 and 20% N_2, by volume. The fuel jet velocity was 151 ± 3 m/s, the fuel exit temperature was 294 K, and the jet Reynolds number was 14,000, based on a mixture viscosity of $\nu=4.85\times10^{-5}$ m^2/s. Laboratory pressure during the experiments was 0.977 atm.

Measurements were made along a radial profile through the jet centerline at a streamwise distance of thirty nozzle diameters (x/d=30), with 600 to 800 shots taken at each radial location. The flame conditions and measurement locations were selected for several reasons. First, the smallest spatial scales for scalar gradients in the flame at this downstream location, as estimated following Smith et al. [22], are larger than the spatial resolution of the system. Second, N_2 dilution reduces the OH levels such that fluorescence trapping effects are small. Third, differential diffusion effects, which are not included in the pdf model, are expected to be modest at this Reynolds number and streamwise location, based on measurements by Smith et al. [22]. Finally, N_2 dilution reduces radiative loss, which can have a significant influence on thermal NO formation in jet flames.

MONTE CARLO PDF PREDICTION

The mean flow field was modeled by a Reynolds stress closure with a downstream marching algorithm [23]. The joint scalar pdf was solved by its modeled transport equation using the Monte Carlo technique [24]. The turbulent transport term was modeled by a gradient diffusion model using the turbulence time and fluctuating velocities from the Reynolds stress model. A modified

Curl's mixing model was used to simulate the effect of turbulent stirring on the molecular diffusion process. The amount of mixing was modeled through a characteristic mixing time, which is related to the turbulence time scale. In the Monte Carlo simulation of the joint scalar pdf, the jet flame is assumed to be axisymmetric and adiabatic. Forty grid points across half of the jet were used, each containing 400 stochastic elements. The time evolution of chemical kinetics for each element was directly computed, using a detailed mechanism for hydrogen combustion with NO_x chemistry, which includes 14 species and 48 steps [25]. The CPU time was about 200 hours on a SGI workstation for calculations up to x/d=150, demonstrating that the inclusion of detailed chemistry in the pdf model is computationally expensive, but not prohibitive. The experimental boundary conditions of nozzle diameter, fuel composition, jet velocity, and coflow velocity were the only inputs to the simulation. Radiation was not included in the present calculation, although radiative heat loss is expected to have some effect on NO formation in this flame, based upon modeling results in similar flames [16]. We do not expect radiative heat loss to have any significant effect on the predicted O-atom concentrations.

RESULTS AND DISCUSSION

The Partial Equilibrium Assumption

The degree of departure from partial equilibrium of the reaction $OH+OH=O+H_2O$ in a hydrogen flame depends on temperature, the local stoichiometry, and the local Damköhler number. Laminar flame calculations and perfectly stirred reactor (PSR) calculations were used to assess the limits of the partial equilibrium assumption for H_2/N_2 combustion in air. These calculations were performed using the chemical mechanism described above. Figure 1 shows the variation with temperature of the ratio $[O]_{peq}/[O]$ in steady strained laminar flames (Tsuji geometry) for three values of the strain parameter; a = 25 s^{-1}, 100 s^{-1}, and 400 s^{-1}. Here $[O]_{peq}$ is the O-atom concentration determined from partial equilibrium according to Eq. (1), and [O] is the actual concentration. Partial equilibrium is achieved within two percent in these laminar flames for temperatures above about 1800 K. In the a=400 s^{-1} flame, $[O]_{peq}/[O]$ reaches 1.05 at about 1500 K and rises rapidly as mixture fraction and temperature decrease on the fuel-lean leg of the curve. Figure 2 shows the ratio $[O]_{peq}/[O]$ versus temperature for PSR calculations at four values of the equivalence ratio from 0.7 to 1.3. A family of curves is generated by decreasing the PSR residence times. For the two fuel-lean cases, $[O]_{peq}/[O]$ exceeds 1.05 at temperatures below about 1450 K. These results from laminar flame and PSR calculations indicate that partial equilibrium is a good assumption for temperatures relevant to thermal NO formation. These calculations also suggest that O-atom concentrations determined from partial equilibrium of the above reaction may significantly exceed the actual O-atom concentrations in fuel-lean mixtures below about 1500 K.

The Monte Carlo pdf simulation itself can be used to assess the applicability of the partial equilibrium assumption for the turbulent flame conditions studied here. This is done in Fig. 3, which is a scatter plot of calculated departure from partial equilibrium versus temperature. Here, departure is defined as the magnitude of the difference between the forward and backward rates divided by the larger of the two rates. For temperatures above ~1400 K most points are close to zero, which corresponds to equal forward and backward rates. Departure from partial equilibrium is less than 5 percent for all but a small number of samples. Based upon the combined results from the laminar flame, PSR, and Monte Carlo calculations, we conclude that the partial equilibrium assumption is valid for the present flame conditions for all temperatures relevant to thermal NO production.

Scatter Plots and Conditional Means

The relationships among scalars in reacting flows can be interpreted effectively when results are plotted in mixture fraction coordinates. For both the experiment and the prediction the mixture

fraction was calculated following the method of Bilger as:

$$f = \frac{(Y_H - Y_{H,2})/w_H - 2(Y_O - Y_{O,2})/w_O}{(Y_{H,1} - Y_{H,2})/w_H - 2(Y_{O,1} - Y_{O,2})/w_O}$$

where the Y's are the hydrogen and oxygen elemental mass fractions, w_H and w_O are atomic weights, and the subscripts 1 and 2 refer to the fuel stream and coflowing air stream, respectively.

Figure 4 shows scatter plots of measured temperature and the major species mole fractions. Conditional averages from the pdf calculation are shown as solid lines, and adiabatic equilibrium conditions are shown as dashed lines. In this flame the temperature and major species are close to equilibrium, except near the stoichiometric mixture fraction, where temperatures and H_2O mole fractions are depressed due to finite rate chemistry. Here, results from the full radial profile are included for both experiment and prediction. In Fig. 5 the conditional means of the measured scalars are compared with the prediction. Agreement for the major species mole fractions is very close. There appears to be a relative shift of about 0.03 in mixture fraction between the measured and predicted conditional mean temperature curves. This shift may be due to differential diffusion, which is not included in the pdf model. Taking the shift into account, the predicted temperatures are slightly higher than measured. This is consistent with the fact that radiation is not included in the present simulation.

In Fig. 6 the experimental scatter data are compared with strained laminar flame calculations at three values of the strain parameter, a, for the Tsuji geometry. These calculations were performed using the same chemical mechanism as for the pdf simulation. They are included to illustrate that the effects of differential diffusion on the temperature and species in the laminar calculations are much greater than in the turbulent flame measurements. Comparing Figs. 4 and 6 we find that differential diffusion in the laminar flames causes broader peaks in the curves of temperature versus mixture fraction, super-equilibrium temperatures in fuel-lean mixtures, and sub-equilibrium temperatures for mixture fraction values greater than about 0.3. Differential diffusion also noticeably alters the shapes of the curves of N_2 and H_2O mole fraction.

Experimental and predicted results for OH, O-atom, NO production rate, and NO mole fraction are compared in Fig. 7. Measurements and pdf results are plotted as scatter points. Here, to minimize the effect of OH fluorescence trapping, we have included only the measurements from the half of the flame profile that was closest to the fluorescence collection optics. The average fluorescence trapping effect near the center of the reaction zone on this side of the flames was determined to be approximately 3 percent, and this small correction has been applied. Curves from the laminar flame calculations and for adiabatic equilibrium are also included in Fig. 7, except in the plot of NO mole fraction. NO mole fractions at equilibrium and in the laminar flames are much higher than in the turbulent flame, and they are not relevant to the discussion that follows. Measured and predicted conditional means of these same scalar quantities are compared in Fig. 8. Note that the jaggedness in the conditional means for the prediction is due simply to statistical noise in the Monte Carlo simulation. In the next paragraphs we will point out some features of the experimental results, discuss similarities and differences between the experiment and the pdf prediction, and contrast these turbulent flame results with the laminar flame calculation.

The experimentally derived O-atom mole fractions in Fig. 7 are consistently above the curve for full adiabatic equilibrium and show greater scatter than does OH. These results are qualitatively consistent with trends of the laminar flames in that the calculated O-atom mole fractions are much more sensitive to strain rate than is the OH mole fraction. The peak in the curve of experimentally derived conditional mean O-atom mole fraction is nearly seven times the maximum value for full equilibrium, whereas the corresponding ratio for OH is less than two.

Agreement between experiment and pdf prediction is relatively good for OH and O-atom mole fractions, with regard to both the qualitative characteristics of the scatter plots in Fig. 7 and the quantitative conditional means in Fig. 8. The peak values of the conditional means are within 10 percent for both OH and O-atom mole fractions. However, the predicted peaks for OH and O-atom align with the equilibrium peaks, whereas the experimental curves are shifted by about 0.1 in mixture fraction in the fuel-lean direction. This difference is believed to be due, at least in part, to differential diffusion, which is not include in the pdf simulation. For mixture fractions below about 0.06 the measured temperatures begin to drop below the range where the partial equilibrium assumption is valid. Consequently, the experimental O-atom results become unreliable. In the context of thermal NO production, this is not a problem because the production rate becomes negligibly small before the partial equilibrium assumption breaks down.

The experimentally derived instantaneous NO production rates are generally greater than the 'equilibrium' rate, which is calculated from adiabatic equilibrium conditions of temperature, [O] and $[N_2]$. However, a significant number of samples fall near or below this 'equilibrium' curve. These samples are believed to correspond to the more highly strained conditions in the flame, where temperature depression counters the superequilibrium O-atom levels. One must also recognize that some of the scatter is due to measurement uncertainty. The predicted scatter plot of NO production rate displays a distinct envelope and has no samples below the 'equilibrium' curve. At present, we are not sure what constraint this envelope represents. In Fig. 8 the peak in the conditional mean NO production rate for the experiment is about 25 percent above the 'equilibrium' curve. The width of the experimental curve at half maximum is twice the width of the 'equilibrium' curve. We note that a previous pdf simulation, which did not include the ambient humidity in the coflowing air, yielded NO mole fractions in very close agreement with the measured conditional mean over the full range of mixture fraction plotted in Fig. 8. This highlights the importance of fully specifying boundary conditions in studies of thermal NO formation, and it highlights the sensitivity of the NO prediction to the small decrease in temperature that results when ambient water vapor is included.

The prediction yields a maximum conditional mean NO production rate that is roughly twice the 'equilibrium' peak, and the width at half maximum is again about twice that of the 'equilibrium' curve. The predicted NO production rate would drop somewhat with the inclusion of radiation, and we are planning to rerun this simulation with a radiation model included. The predicted conditional mean NO mole fraction is lower than measured, even though the predicted NO production rate is higher. This is consistent with our understanding of trends in the pdf simulations. In previous simulations of jet flames [18, 26], the pdf model severely underpredicted NO formation near the base of the flames, but overpredicted NO levels higher in the flames when the simulations were adiabatic. At the present location of x/d=30 the NO levels have not yet recovered from underprediction near the flame base, but the predicted production rates are high enough in this adiabatic simulation to eventually cause an overprediction of the total NO emission.

Comparison of laminar flame calculations with the experimental results in Fig. 7 reveals that it would not be possible to represent the turbulent flame behavior using any combination of these steady laminar flames. OH levels in the laminar flames are significantly higher than both the measurements and the pdf model predictions. O-atom levels for strain rates below $a=100\ s^{-1}$ are consistent with the experimental results. However, the NO production rates for these weakly strained flames far exceed the experimentally derived production rates. Two issues are involved here. First, the degree of differential diffusion in the laminar flames appears to be much greater than in the turbulent. In weakly strained flames this produced temperatures that are above equilibrium, and the resulting thermal NO production rates are unrealistic in the context of turbulent combustion. Second, a steady one-dimensional laminar flame only admits a single time fluid-dynamic time scale, which is equal to the reciprocal of the specified strain rate and is, arguably, analogous to a local strain rate in a turbulent flame. Laminar flames, as calculated here, cannot account for the convective time scale in turbulent flames, which is associated with process

of radical recombination. This limitation dictates that a flamelet calculation based upon a library of conventional steady laminar flame will overpredict the radical concentrations in the downstream portion of a turbulent jet flame.

Radial Profiles

Radial profiles of ensemble-average temperature and species mole fractions are shown in Fig. 9, and we find that agreement between measured and predicted results for temperature, the major species, OH, and O-atom is not as good for these spatial profiles as it was when data were considered in mixture fraction coordinates. The predicted temperature profile is significantly broader than the measured profile. The predicted H_2 mole fraction on the centerline is higher than measured, and the predicted centerline temperature is lower. Within the reactions zones (near r/d = $\pm$2.5) the predicted OH and O-atom mole fractions are below the measured curves. (Note that the OH profile in Fig. 9 was not corrected for the effect of fluorescence trapping and the OH peak on the positive side is about 7 percent lower than on the negative side, which was closer to the collection optics.) These results show that, while the model predicts the chemistry reasonably well, it over-predicts the turbulent mixing rates, such that the flame spreads too rapidly, and the pdf's of mixture fraction in the reaction zones are too broad.

CONCLUSIONS

1. We have demonstrated an experimental procedure for determining oxygen atom concentrations and instantaneous thermal NO production rates in turbulent flames. This procedure is based upon simultaneous point measurements of temperature, the major species, and OH, and it may be applied wherever the assumption of partial equilibrium of the reaction $OH+OH=O+H_2O$ is valid.

2. Measurements were made across a radial profile at a single streamwise location, 30 nozzle diameters from the base of a turbulent jet flame of nitrogen-diluted hydrogen. The partial equilibrium assumption was shown to be valid in this flame for temperatures greater than about 1500 K. Instantaneous and conditionally-averaged O-atom mole fractions at this measurement location are significantly greater than equilibrium levels. The conditional mean of the experimentally derived O-atom mole fraction has a peak nearly seven times the full equilibrium value. The width in mixture fraction coordinates of the curve of the conditional mean NO production curve is roughly twice the width of the production rate calculated from adiabatic equilibrium conditions of temperature, [O], and $[N_2]$.

3. Experimental results were compared with predictions by the Monte Carlo pdf model using detailed chemistry. For temperature, the major species, OH and O-atoms, there is generally good agreement between measurements and predictions when results are considered in mixture-fraction coordinates (scatter plots and conditional means). Agreement is not as good when radial profiles of ensemble-average scalars quantities are compared. This indicates that the present pdf model predicts the hydrogen and nitrogen chemistry with good accuracy, but that improvements are needed in the modeling of the turbulent fluid dynamics and mixing. The predicted NO production rates are higher than those determined from the experiments, due in part to the fact that radiation was not included in the model.

4. This experimental approach constitutes an important new tool for investigating the effects of turbulence-chemistry interactions on O-atom superequilibrium in flames and for developing a more complete understanding of the role of turbulence-chemistry interactions in thermal NO formation. Results may also be used to evaluate a wide range of turbulent combustion models.

Acknowledgments

This research was supported by the United States Department of Energy, Office of Basic Energy Sciences, Division of Chemical Sciences. The contributions of T. Prast in support of the laboratory experiments are gratefully acknowledged.

REFERENCES

1. Correa, S. M., *Comb. Sci Tech.* 87:329-362 (1992).
2. Kent, J. H., and Bilger, R. W., *Fifteenth Symposium (International) on Combustion*, The Combustion Institute, Pittsburgh, 1974, p. 1643.
3. Lavoie, G. A., and Schlader, A. F., *Comb. Sci Tech.* 8:215-224 (1974).
4. Bilger, R. W., and Beck, R. E., *Sixteenth Symposium (International) on Combustion*, The Combustion Institute, Pittsburgh, 1976, p. 541.
5. Drake, M. C., Correa, S. M., Pitz, R. W., Shyy, W., and Fenimore, C. P., *Combust. Flame* 69:347-365 (1987).
6. Vranos, A., Knight, B. A., Procia, W. M., and Chiapetta, L., *Twenty-Fourth Symposium (International) on Combustion*, The Combustion Institute, Pittsburgh, p. 377, 1992.
7. Turns, S. R., and Lovett, J. A., *Comb. Sci Tech.* 66:233-249 (1989).
8. Turns, S. R., and Myhr, F. H., *Combust. Flame* 87:319-335 (1991).
9. Driscoll, J. F., Chen, R.-H., and Yoon, Y., *Combust. Flame* 88:37-49 (1992).
10. Carter, C. D., and Barlow, R. S., *Optics Letters* 19:299-301 (1994).
11. Barlow, R. S., and Carter, C. D., *Combust. Flame* 97:261-280 (1994).
12. Barlow, R. S., and Carter, C. D., *Relationships Among Nitric Oxide, Temperature, and Mixture Fraction in Hydrogen Jet Flames, Combust. Flame*, (in press).
13. Meier, W., Vyrodov, V., Bergmann, W., and Stricker, W., *Simultaneous Raman/LIF Measurements of Major Species and NO in Turbulent H_2/Air Diffusion Flames, Appl. Phys. B* (to appear).
14. Nguyen, Q. V., Dibble, R. W., Carter, C. D., Fiechtner, G. J., and Barlow, R. S., *Laser Measurements of Temperature, the Major Species, OH, and NO in a Methane-Air Bunsen Flame, Combust. Flame* (to appear).
15. Dally, B. B., Masri, A. R., Barlow, R. S., Fiechtner, G. J., and Fletcher, D. F., *Measurements of NO in Flames Stabilized on a Bluff Body*, submitted to the *Twenty-Sixth Symposium (International) on Combustion.*
16. Smith, N. S. A., Bilger, R. W., Barlow, R. S., Carter, C. D., and Chen, J.-Y., *Radiation Effects on Nitric Oxide Formation in Turbulent Hydrogen Jet Flames Diluted with Helium*, (submitted).
17. Goldsmith, J. E .M., *Appl. Optics* 26:3566-3572 (1987).
18. Smyth, K. C., and Tjossem, P. J. H., *Appl. Phys. B* 50:449-511 (1990).
19. Paul, P. H., *J. Quant. Spectrosc. Radiat. Transfer* 51:511-524 (1994).
20. Paul, P. H., Gray, J. A., Durant Jr., J. L., and Thoman Jr., J. W., *AIAA J.* 32:1670-1675 (1994).
21. Barlow, R. S, and Fiechtner, G. J., paper in preparation.
22. Smith, L. L., Dibble, R. W., Talbot, L., Barlow, R. S., and Carter, C. D., *Combust. Flame* 100:153-160 (1995).
23. Chen, J.-Y., Kollmann, W., and Dibble, R. W., *Comb. Sci Tech.* 64:315-346 (1989).
24. Pope, S. B., *Comb. Sci Tech.* 25:159-174 (1981).
25. Gutheil, E., Balakrishnan, G., and Williams, F. A., in *Reduced Reaction Mechanisms*, (N. Peters and B. Rogg, Eds.) *Lecture Notes in Physics*, 15, Springer-Verlag, 1993, pp. 177-195.
26. Smith, N. S. A., Bilger, R. W., Carter, C. D., Barlow, R. S., and Chen, J.-Y., *Combust. Sci. Tech.* 105:357-375 (1995).

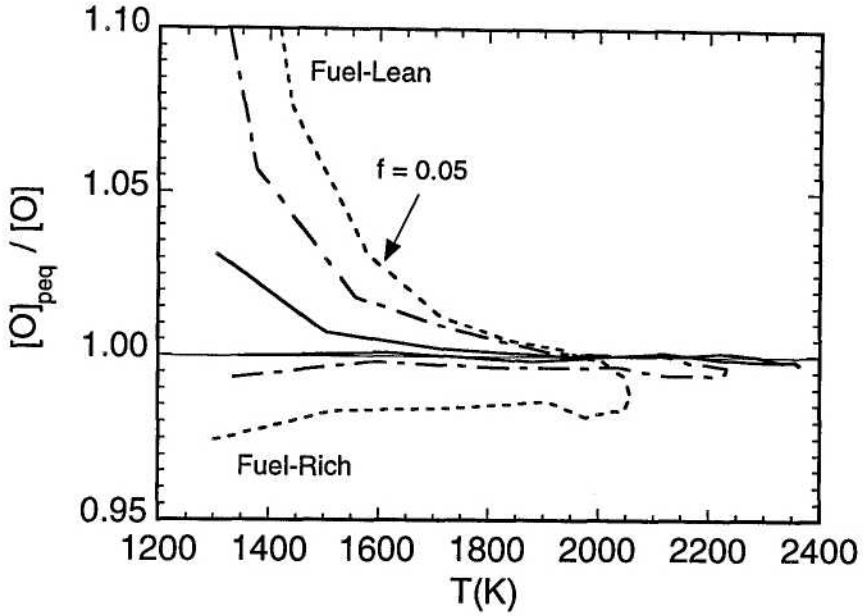

Fig. 1. Ratio of partial-equilibrium O-atom concentration to actual O-atom concentration plotted versus temperature for steady strained laminar flame calculations at values of the strain parameter, a, of 25 s^{-1} (———), 100 s^{-1} (— — —), and 400 s^{-1} (------).

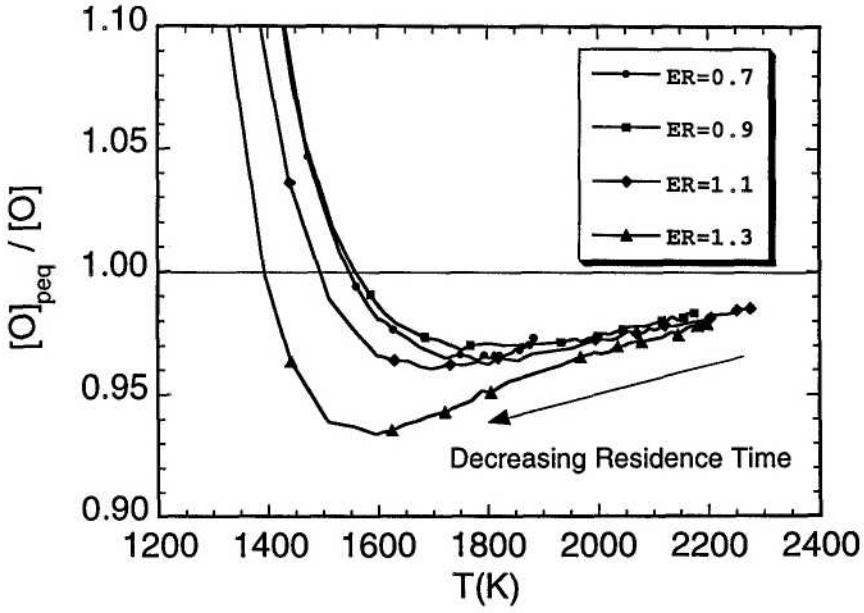

Fig. 2. Ratio of partial-equilibrium O-atom concentration to actual O-atom concentration plotted versus temperature for perfectly stirred reactor calculations with varying residence times at equivalence ratios of 0.7, 0.9, 1.1, and 1.3.

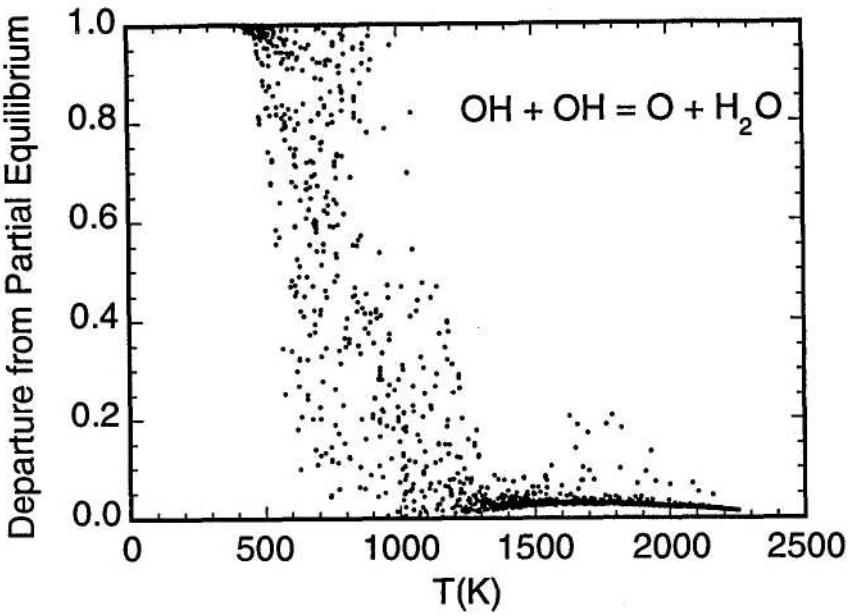

Fig. 3. Scatter plot of departure from partial equilibrium of the reaction OH+OH=O+H2O versus temperature derived from the pdf model simulation at x/d=30.

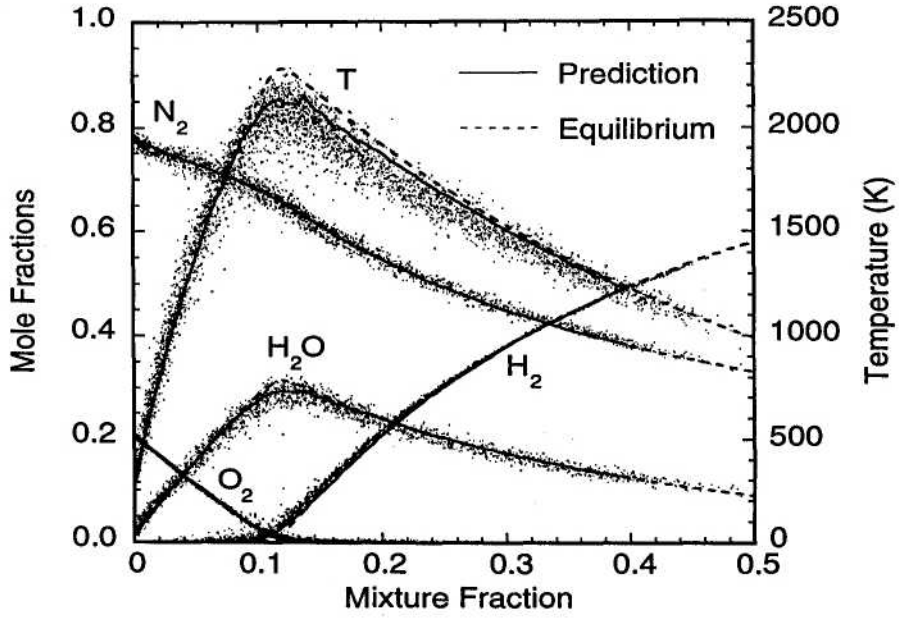

Fig. 4. Comparison of measured temperature and major species mole fractions (scatter points) with conditional averages from the pdf model prediction (——) for the streamwise location of x/d=30. Adiabatic equilibrium curves (------) are also included.

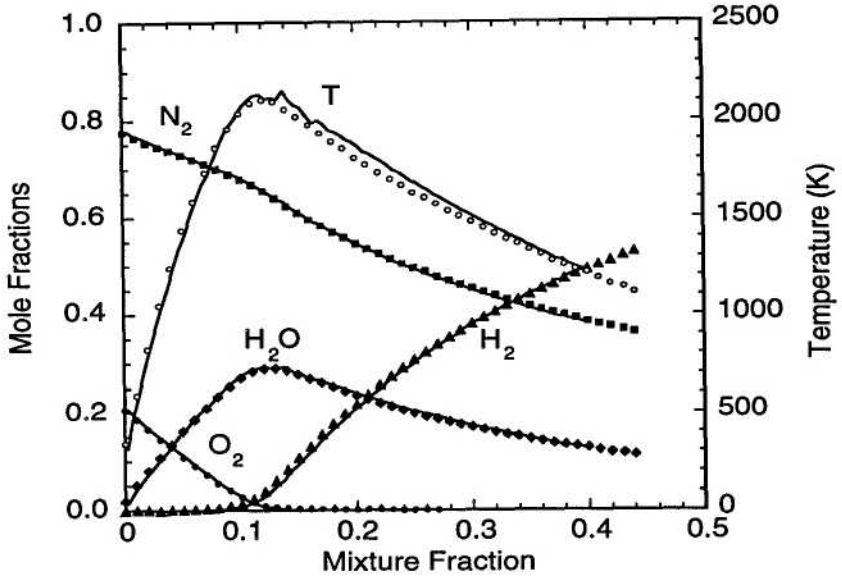

Fig. 5. Comparison of conditional averages of measured temperatures and major species mole fractions (symbols) with the same predicted conditional means (——) as in Fig. 2.

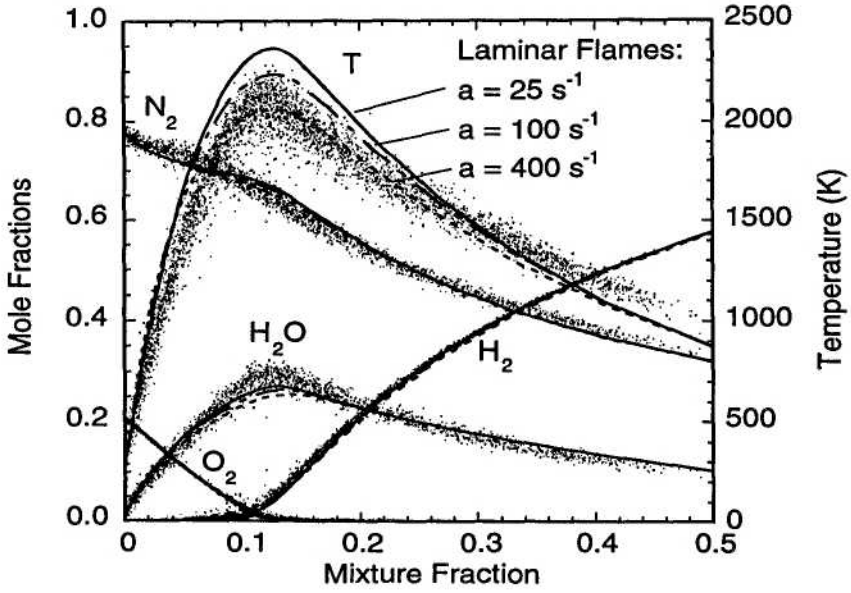

Fig. 6. Comparison of measured temperature and major species mole fractions (scatter points) with results from steady laminar flame calculations for values of the strain parameter, a, of 25 s^{-1} (——), 100 s^{-1} (— — —), and 400 s^{-1} (------).

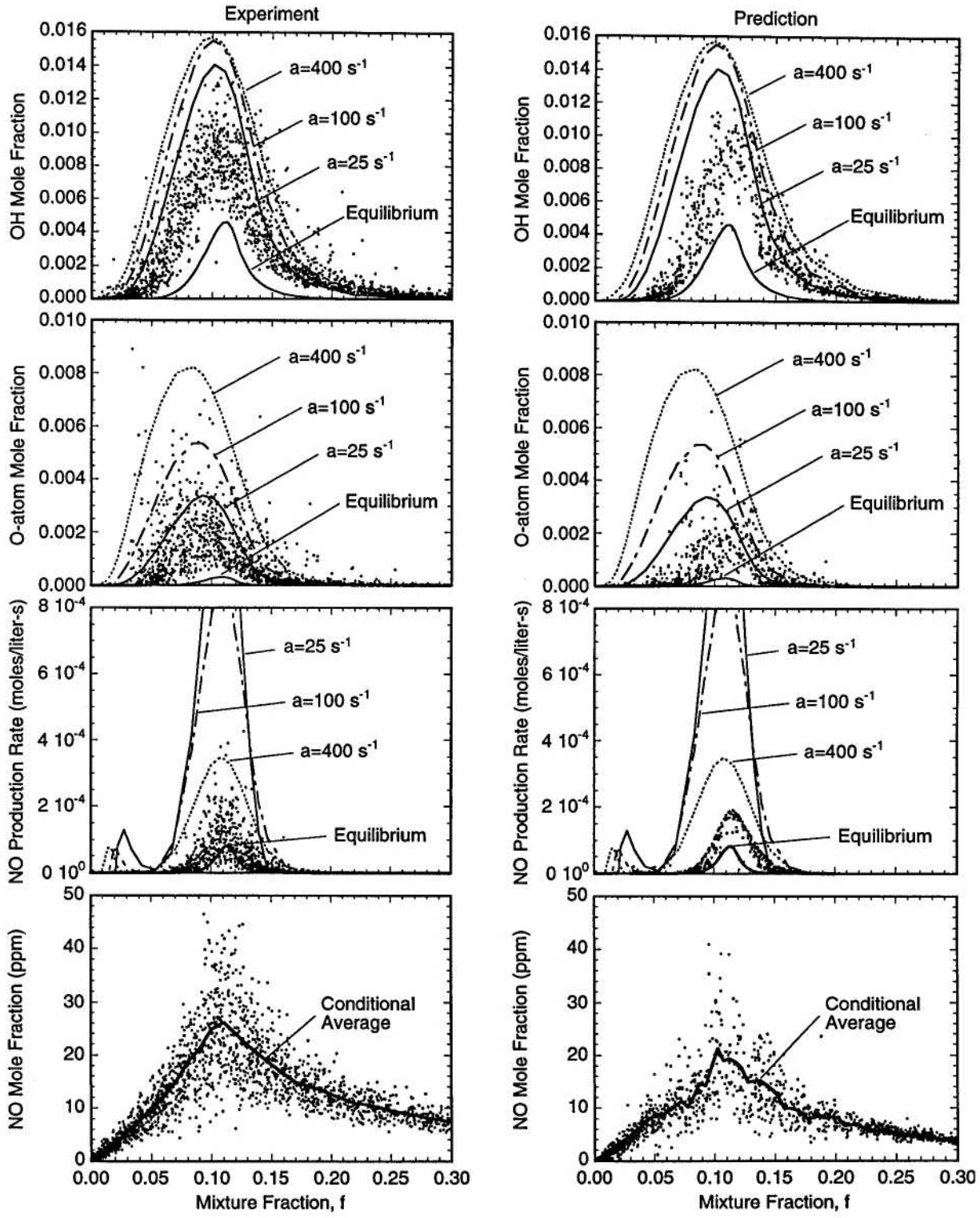

Fig. 7 Scatter plots of experimental and predicted results for OH mole fraction, O-atom mole fraction, thermal NO production rate, and NO mole fraction at x/d=30. Adiabatic equilibrium curves and results of laminar flame calculations at a=25 s^{-1}, a=100 s^{-1}, and a=400 s^{-1} are included.

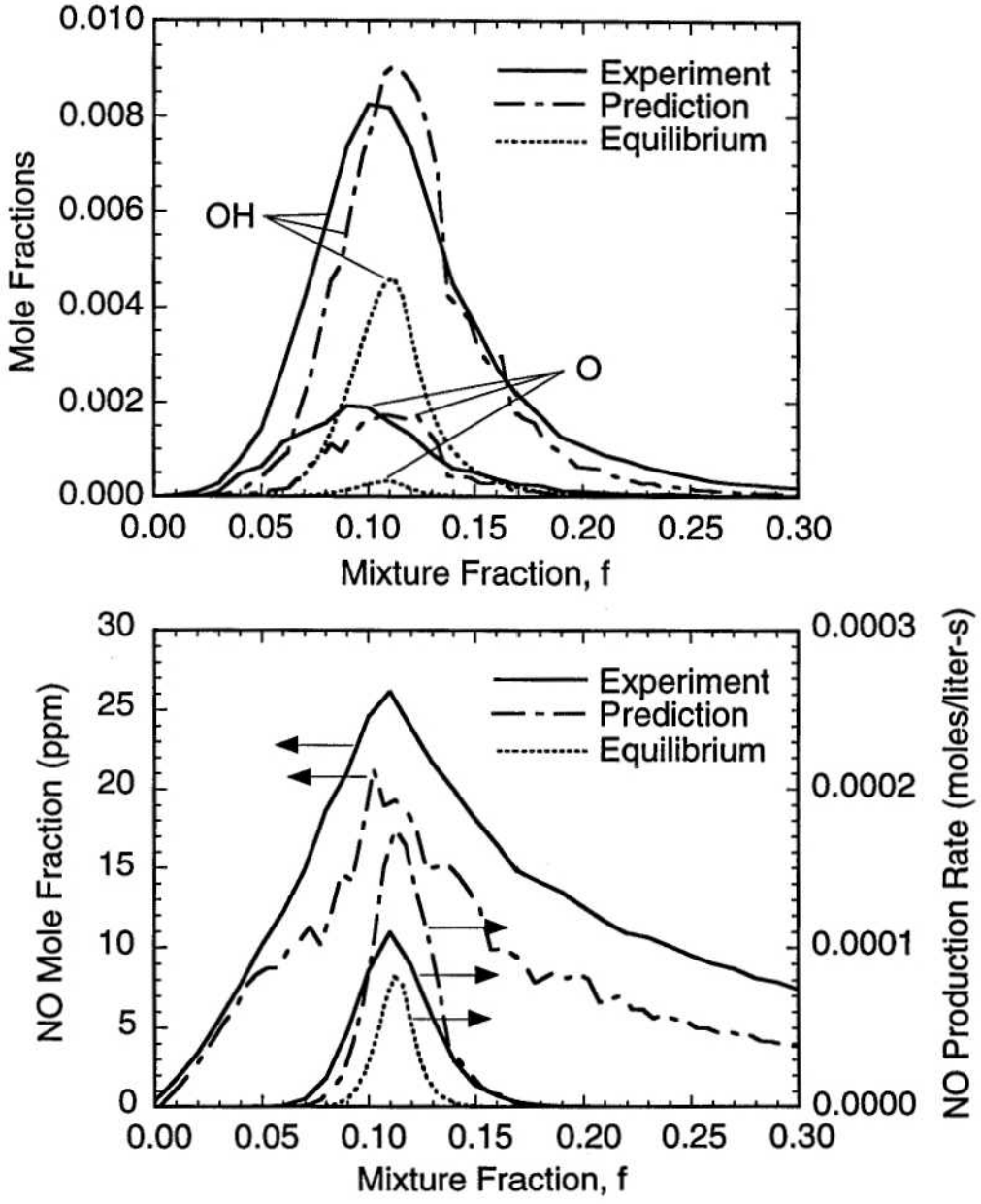

Fig. 8. Experimental (——) predicted (— — —) conditional means plotted together with adiabatic equilibrium versus mixture fraction and adiabatic equilibrium of OH mole fraction, O-atom mole fraction, thermal NO production rate, and NO mole fraction at x/d=30. (——), 100 s^{-1} , and 400 s^{-1} (------).

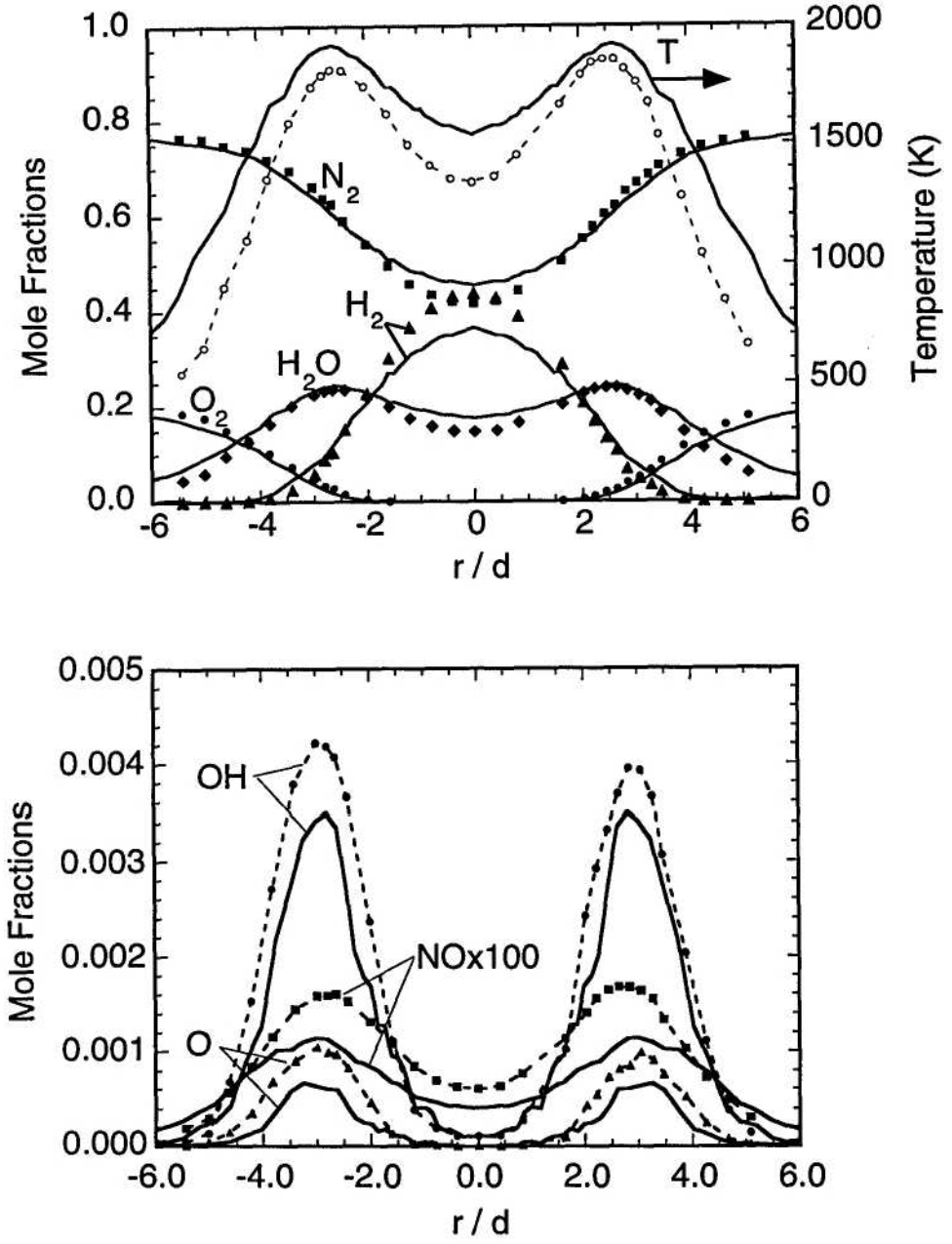

Fig. 9. Radial profiles of ensemble-average temperature and species mole fractions from the experiment (symbols) and the prediction (——) at x/d=30. The difference between the two OH peaks is due to fluorescence trapping.